Edge-preserving Filtering and Fuzzy Image Enhancement in Depth Images Captured by Realsense Cameras in Robotic Applications

Vladimir TADIC, Akos ODRY, Ervin BURKUS, Istvan KECSKES, Zoltan KIRALY, Peter ODRY
University of Dunaujvaros, Tancsics Mihaly u. 1/A Pf.: 152, 2401. Dunaujvaros, Hungary
tadityv@uniduna.hu

***Abstract*—This paper presents both the use of depth cameras in robotic applications and effects of post-processing on the captured depth images. The performance of depth cameras and post-processing image enhancement are evaluated with the aim to improve the depth-based object detection. First, the edge-preserving exponential moving average (EMA) filter and the fuzzy contrast enhancement procedures are briefly introduced. Then, the use of depth cameras with post-processing methods is shown in the example of painting robots. The use of the stereo depth camera is essential in robotic applications, since it constitutes the initial steps in a series of robotic operations, where the goal is to both detect and extract obstacles on walls that are not intended to be painted.**

***Index Terms*—filtering algorithms, fuzzy logic, image enhancement, robots, stereo vision.**

I. INTRODUCTION

This paper presents a robotic application based on depth image processing captured using low-cost RealSense stereo camera [1 – 5]. This work is a part of an industrial-research project aiming to construct a robot that would automatically, based on information obtained from the depth camera [6 - 10], paint the buildings facades. The task is to develop a robust and simple algorithm with simple image processing operations that would both detect and extract the obstacles on walls using depth images recorded with stereo camera and notify the controlling system [11 – 16]. This paper introduces the procedures for enhancement of the depth images to facilitate the obstacle detection and extraction from the image background. The first enhancement step is the edge-preserving filtering with an exponential moving average filter. This filtering method both lifts and preserves the edges of the objects in the depth image [17 – 22]. The next step in the algorithm is the fuzzy contrast enhancement owing to the depth image background variation in gray levels. The reason for these operations is to facilitate and improve the obstacle detection in the depth image. Finally, the obstacle is detected and extracted using binary morphological operations.

II. RELATED WORK

This section will give a brief review of related work. There are many edge enhancing techniques in practice, but not all of them are suitable for robotics application. For example, in most cases real time techniques are needed, therefore algorithms that require a longer processing time must be avoided.

Gastal and Oliveira [12] presented an approach for performing a high-quality edge-preserving filtering of images and videos in real time. Their solution relies on a transform that defines an isometry between curves on the 2D image manifold in 5D and the real line. It is shown that this transform preserves the geodesic distance between points on these curves, adaptively warping the input signal so that the 1D edge-preserving filtering can be efficiently performed in linear time. Garnica et al. [23] introduced a new method to edge-preserving smoothing of the digital images, where it was shown that the developed algorithm overcomes some of the disadvantages of the existing smoothing filters and is conceived as an extension of the edge-preserving Maximum Homogeneity Neighbor Filter. The proposed procedure cleans up the image noise in the homogeneous areas but preserves all relevant image structures like edges or corners. Reich et al. [24] introduced a filter that removes a wide variation of noise but preserves the edges in the image. The filter performance was evaluated on Berkeley Image Dataset and Coco Dataset, and it is considered adequate for robotics applications. Abiko and Ikehara [25] proposed a novel method for edge preserving smoothing filtering. The introduced procedure uses a 2D filter to smooth images and then an indicator function is applied to restrict the range of filtered pixels for edge-preservation. To define the indicator function, the distance between each pixel is recalculated using the edge information. The nearby pixels were used for image smoothing in the new domain. Choi et al. [26] developed a new pan-sharpening framework for improvement of the spatial clarity of very high-resolution satellite images. The proposed algorithm aims to remove the spatial dissimilarity between panchromatic and multispectral images using the guided filtering algorithm and to generate the optimal local injection gains for pan-sharpening process. Iqbal et al. [27] introduced an adaptive noise detector and a new weighted mean filter for removing the random-valued impulse noise from the images. In contrast to other noise detectors, the introduced detector computes a new and adaptive threshold for each pixel. The detection accuracy is further improved by employing edge identification stage to ensure that the edge pixels are not incorrectly detected as noisy pixels. The experimental results showed that the new method outperforms all the state-of-the-art noise detection procedures in suppressing random valued impulse noise. Zhu et al. [28] proposed a benchmark for edge-preserving image smoothing. This benchmark includes an image

This research has been funded by projects EFOP-3.6.1-16-2016-00003 and KFI_16-1-2017-0485, co-financed by the European Union.

Digital Object Identifier 10.4316/AECE.2020.03010

dataset with ground truth image smoothing results as well as baseline algorithms that can generate competitive edge-preserving smoothing results for a wide range of image contents. They trained a deep convolutional neural network to design a loss function for edge-preserving smoothing which runs faster than most state-of-the-art smoothing algorithms with leading smoothing results both qualitatively and quantitatively. Samrudh and Sandeep [29] developed a new fuzzy system to enhance the contrast of the low-resolution images overcoming the shortcomings of the traditional methods. They have highlighted the significant improvements of the image contrast. Van De Ville et al. [30] proposed a new fuzzy filter for the noise reduction of images corrupted with additive noise. The fuzzy filter consists of two stages; the first stage computes a fuzzy derivative for eight different directions and the second stage uses these fuzzy derivatives to perform fuzzy smoothing by weighting the contributions of neighboring pixel values. Both stages are based on fuzzy rules which utilize the fuzzy membership functions. They have made a series of experiments and the obtained results showed the feasibility of the proposed approach. Cheng and Xu [31] proposed an adaptive direct fuzzy contrast enhancement method based on the fuzzy entropy principle and the fuzzy set theory. They have conducted experiments on large image database. The experimental results have demonstrated that the developed algorithm is very effective in contrast enhancement as well as in preventing over-enhancement too. Parihar et al. [32] proposed a contrast enhancement algorithm based on fuzzy contextual information of the images. They have introduced a fuzzy similarity index and fuzzy contrast factor to capture the neighborhood characteristics of a pixel. The detailed experiments and analysis showed that the proposed algorithm efficiently enhances the contrast and yields natural image appearance. Tadic et al. [33] presented a license plate detection algorithm based on fuzzy image filtering. It was noted that the new algorithm is very robust and resistant to noise. Salih et al. [34] proposed a specifically designed method for contrast enhancement using specific algorithms for different regions. Parihar [35] introduced a fuzzy contrast distribution (FCD) algorithm that computes an FCD of the input image using fuzzy membership function and fuzzy rules. An adaptive parameter gamma is defined using the FCD. The proposed algorithm uses the gamma correction with adaptive gamma to obtain the contrast enhanced images. He stated that the developed algorithm yields a good contrast and natural looking images.

III. The Technology of Intel RealSense Cameras

Recently, computer vision applications based on 2D image processing have been largely limited due to a lack of information on the third dimension, i.e. depth. Unlike 2D vision, 3D vision makes it possible for computers and other machines to differentiate accurately and with great precision various shapes, shape dimensions, distances, and control in the real, three-dimensional world [1 – 4].

A few years ago, Intel introduced its own family of depth cameras, Intel RealSense cameras. The RealSense technology consists of a processor for image processing, a module for forming depth images, a module for tracking movements and of depth cameras. These cameras rely on deep scanning technology, which enables computers to see objects in the same way as humans.

RealSense cameras have three lenses: a conventional RGB (Red Green Blue) camera, an infrared (IR) camera and an infrared laser projector. All three lenses jointly make it possible to assess the depth by detecting the infrared light that has reflected from the object/body that lies in front of it. The resulting visual data, combined with the RealSense software, create a depth estimate, i.e. provide a depth image.

RealSense cameras use stereovision to calculate depth. The implementation of stereovision consists of a left-side and a right-side camera, i.e. sensors, and of an infrared projector. The infrared projector projects invisible IR rays that enhance the accuracy of the depth information in scenes with weak textures. The left-side and right-side cameras record the scene and send data about the image to the processor that, based on the received data, calculates the depth values for each pixel of the image, thus correlating the points obtained with the left-side camera to the image obtained with the right-side camera [7 – 9].

The value of the depth pixel describing the depth of an object is determined in relation to a parallel plane of the camera doing the recording, and not in relation to the actual distance of the object from the camera [7].

The performance and affordable cost are the advantages that make these cameras popular choice in numerous devices that require high-speed data processing camera [10 – 14].

IV. Edge Preserving and Fuzzy Depth Image Enhancement

The task associated with the RealSense depth cameras can be divided into the following steps:

1. Capturing images of part of the building
2. Detecting the obstacles in the wall that must not be painted
3. Forwarding the information about the coordinates of the obstacle to the robot
4. Painting part of the building by bypassing the detected obstacles.

The main requirements of a project client were to develop an algorithm that would separate the wall from the windows on the facades using low-cost equipment. Only rectangular, semi-circular, vaulted and circular windows are considered by the client. Hence, the previously mentioned various shaped windows are the real obstacles in the real-time processing. There are not considered any other type of shapes and obstacles by the client.

The painting robot is shown in Fig. 1. Since the process of developing and testing of the mentioned robot is still in its building phase, the experiments have been conducted with artificially created obstacles followed by examples with a walls and windows simulated a real situation. The goal of testing with undefined shaped obstacles is to present the capabilities of the depth camera and the obstacle detection algorithm. Because in robotics a high degree of accuracy and precision are required, the depth cameras need to be calibrated in the appropriate manner, so that the obstacle is clearly visible and can be detected in a complex image. There are numerous parameters and conditions that affect

the quality of the depth image such as noise, light, sunlight, darkness, etc.

Since the depth difference is almost always present between walls and windows, the use of the depth camera is an essential step of the image processing algorithm. Therefore, the low-cost RealSense D415 depth camera has been chosen for depth measurements. The depth camera and their settings are easily controlled via Robotic Operating System (ROS). The users can choose and save specific settings in the camera software for various recording conditions such as variable luminosity, shadow, etc. Also, there are available various built-in settings for the accuracy settings and for various recording conditions of a depth measurement. A well measured and recorded depth image distinguishes the wall from window very well in most situations [7 – 11].

In the end, the image processing algorithm will be fused with the camera's ROS wrapper software [7] and the complete process will be embedded in robot's controlling system using ROS.

Many higher-level applications definitely need the high depth accuracy and low depth noise and therefore the measured depth images need additional post-processing to improve their depth accuracy. The main improvements of the depth images are the edge preserving and the contrast enhancement to distinguish the obstacle from the background based in depth information.

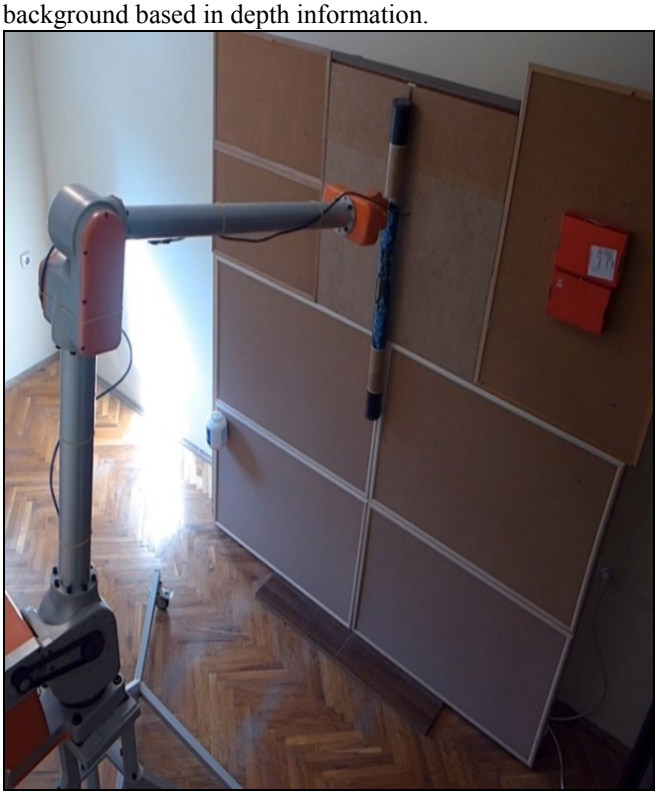

Figure 1. The painting robot in testing process

V. Edge-Preserving Exponential Moving Average Filter

In this section, the edge-preserving EMA filter will be introduced in brief. This type of filter will smooth the depth noise while attempting to preserve edges in the depth image. This filter is built in the RealSense *librealsense* [7] software package.

During image processing, a single 3D image, a point cloud is used to derive the depth information.

As the depth measurement are noisy, the goal is to preserve the edges to facilitate extraction of the obstacle from the background.

The used edge-preserving filter is a type of infinite impulse response (IIR) filter. For this filter, the depth map was raster scanned in X-axis and Y-axis and back again, twice, while calculating the one-dimensional EMA using an alpha parameter that determines the amount of smoothing [39], [40]. The alpha is a damping parameter which controls the filter's attenuation [7], [39 - 40]. The specific recursive equation for this filter is:

$$S_t = \begin{cases} Y_1, & t = 1 \\ \alpha Y_{t-1} + (1-\alpha) S_{t-1}, & t > 1, \Delta = |S_t - S_{t-1}| < \delta_{thresh} \\ Y_{t-1}, & t > 1, \Delta = |S_t - S_{t-1}| > \delta_{thresh} \end{cases} \quad (1)$$

The α coefficient represents the degree of weighting decrease, the Y_t is the newly recorded instantaneous value (of the disparity or of the depth), and S_t is the value of the EMA at any time of the period *t*.

When $\alpha = 1$ no filtering is performed and the output is just equal to the input, while $\alpha = 0$ means an infinite history of filtering, i.e. the α determines the depth of memory of the EMA filter [40]. Also, there is an additional threshold parameter denoted as δ_{thresh}. If the depth value between neighboring pixels exceeds the depth threshold set by this delta parameter, α will be temporarily reset to 1, i.e. filtering step would be omitted and edges would not be preserved [8]. This means that if an edge is observed, then the smoothing is temporarily turned off. This will cause artefacts depending on whether the edge was moved across from the right-to-left or left-to-right, which is why the filtering is typically employed in two bi-directional passes in both *x* and *y* directions, which tends to be enough to reduce the artefacts in the depth image [8]. Further, care should be taken to use the parameters that do not remove features over-aggressively because the aggressive filtering could distort the depth image [8].

The EMA smoothing filter scheme will be discussed in brief since the edge-preserving operation is the most important for the successful obstacle extraction from the captured depth images.

The next formulation of the mentioned algorithm is introduced by Hunter [40]. The exponentially weighted moving average (EWMA), or otherwise EMA has been introduced a long time ago, but with the development of digital signal processing it has gained prominence in some applications, i.e. the edge-preserving and noise reduction. The smoothing scheme begins by setting values S_2 and Y_1, where S_i is the smoothed observation of EWMA and Y is the original observation. The subscripts refer to the time periods, *t=1, 2, ..., n*. For example, the equation for the third period is:

$$S_3 = \begin{cases} Y_1, & t=1 \\ \alpha Y_2 + (1+\alpha)S_2, & 0<\alpha\le 1, t\ge 3, \Delta = |S_t - S_{t-1}| < \delta_{thresh} \\ Y_2 & 0<\alpha\le 1, t\ge 3, \Delta = |S_t - S_{t-1}| > \delta_{thresh} \end{cases} \quad (2)$$

and so on. There is no S_1, the smoothed series, the image filtering starts with the smoothed version of the second observation. The basic equation of the exponential smoothing is given by expression (1). The initial EWMA plays an important role in computing all the subsequent EWMAs. There are several initialization options for setting the S_2: it could be equal to Y_1, equal to the target of the process, or present average of the several initial observations. It can be shown that if α is set to a small value, the selection of initial EWMA has more influence on the results. Further, let the basic equation be expanded by substituting for S_{t-1} to obtain S_t:

$$S_t = \alpha Y_{t-1} + (1-\alpha)\left[\alpha Y_{t-2} + (1-\alpha)S_{t-2}\right] \quad (3)$$

If substituting for S_{t-2}, then for S_{t-3}, and so forth, until S_2 (which is just Y_1) is reached, it can be shown that the expanding equation can be written as:

$$S_t = \alpha \sum_{i=1}^{t=2} (1-\alpha)^{i-1} Y_{t-i} + (1-\alpha)^{t-2} S_2, \quad t \ge 2 \quad (4)$$

The expanded expression for the smoothed value of S_5 is:

$$S_5 = \alpha\left[(1-\alpha)^0 Y_4 + (1-\alpha)^1 Y_3 + (1-\alpha)^2 Y_2\right] + (1-\alpha)^3 S_2 \quad (5)$$

The expression (5) illustrates the exponential behavior. The weights, $\alpha(1-\alpha)t$ decrease geometrically and their sum is unity and they have a property of geometric series:

$$\alpha \sum_{i=0}^{t-1} (1-\alpha)^i = \alpha\left[\frac{1-(1-\alpha)^t}{1-(1-\alpha)}\right] = 1-(1-\alpha)^t \quad (6)$$

From the equation (6) it can be seen that the summation term shows that the contribution to the smoothed value S_t becomes smaller in each following consecutive time instant.

The current EWMA value depends on all the previous, historical information and there is no need to keep records of the previous observations or their weights.

The EMA filter is beneficial in real time applications for two reasons. First, it is easy to adjust the cutoff frequency. Decreasing the value of α will lower the cutoff frequency of the filter. Second, the EMA is easy to code and requires only a small amount of computing power. Therefore, the RealSense engineering team have chosen this EMA filter to implement it in the camera's software package. For facades with variable luminosity contrast, the EMA filter can be adjusted during measurement in the RealSense software via ROS to obtain satisfactory edges in the depth image [7 – 11]. Moreover, all the parameters of the depth camera can be easily adjusted in the RealSense software via ROS interactively [7].

The EMA filter is one of numerous options for an edge-preserving filtering. It is also possible to try the edge-preserving with guided filter, high-pass filter, bilateral filter, anisotropic diffusion, etc.

The improvement after the smoothing, filtering is obvious from Fig. 2. Fig. 2. (a) shows the cross-section of the desired depth image with ideally presented edges. Fig. 2. (b) shows the real situation after depth measurement. The depth image and the edges in the image are highly damaged with noise due to the measuring conditions. Finally, Fig. 2. (c) shows the EMA filtered image. It is noticeable that the edges are preserved with little interference and the strong noise is eliminated. These interferences can be easily eliminated with further post-processing.

VI. Enhancements of the Depth Image using the Fuzzy Logic

The edge-preserving filter made huge quality improvements in the measured depth image, but still there are some issues which can cause problems in obstacle extraction. Namely, the background of the obstacle always contains noise and various gray ambiguous image components which makes it difficult to extract the obstacle from the wall background. This illumination problem is caused by the RealSense camera sensor and lighting conditions, and it can be fixed with contrast improvement. Since the illumination of the background is very stochastic and unpredictable, the fuzzy logic is chosen for the solution of this problem.

Fuzzy image processing and enhancement is based on gray-level mapping from a gray plane into a fuzzy plane using membership functions [33]. It uses the principle of contrast stretching where the image gray levels are transformed in such a way that dark pixels appear darker and bright pixels appear much brighter in the image.

The pixels with intensities principle of contrast stretching depends on the selection of the threshold *t*, so that the gray levels below the threshold *t* are reduced and *t*he gray levels above the threshold *t* are increased in a nonlinear manner. This stretching operation induces saturation at both ends of the gray levels. Generally, this can be expressed with the following equation [41] pages [47-49]:

$$contrast(x) = \begin{cases} (1-a)x, & x > t \\ x, & x = t \\ (1+b)x, & x > t \end{cases} \quad (7)$$

where t is the threshold, contrast(x) is an intensifier contrast stretching that transforms the gray level x to an intensified level, and a and b are the values between 0 and 1 that decide a stretching percentage of the x level for an certain t threshold. This solution can be extended to multiple thresholds where different regions of the image are stretched in different ways depending on the quality of an image like in the example later in this section.

Image contrast can be improved by using human knowledge. The quality evaluation by the human observer is highly subjective in nature. Different observers judge the image in different ways. Fuzzy rule–based approach is such a method that incorporates human intuitions that are nonlinear in nature. As it is difficult to define a precise or crisp condition under which enhancement is applied, a fuzzy set theoretic approach is a method of choice. A set of conditions are defined on a pixel for image enhancement and these conditions will form the antecedent part of the IF–THEN rules. The conditions are related to the pixel gray level and also to the pixel neighborhood.

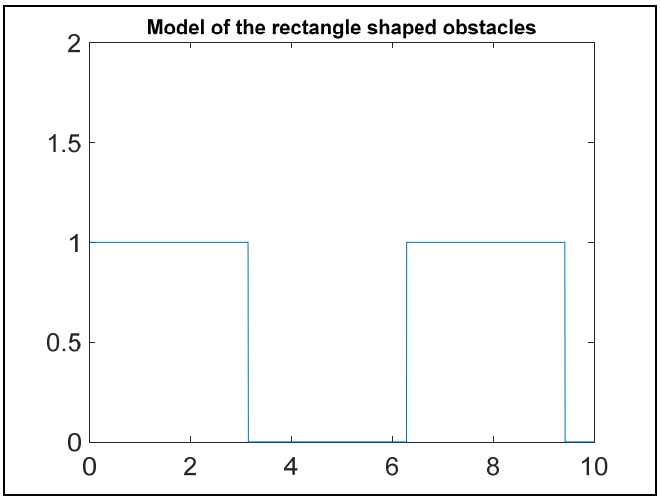

(a)

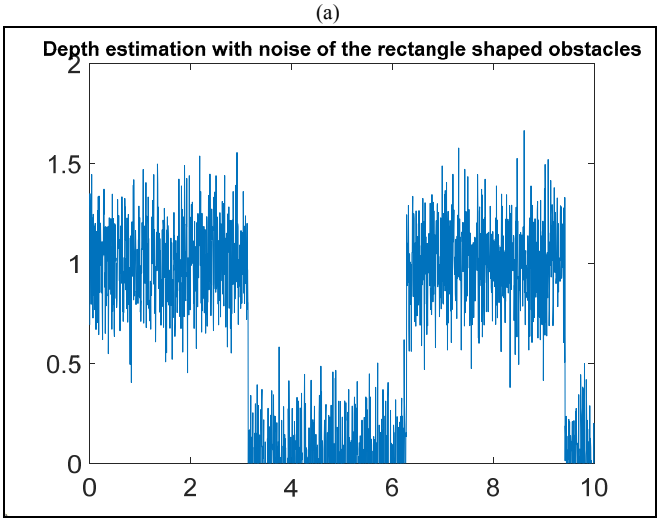

(b)

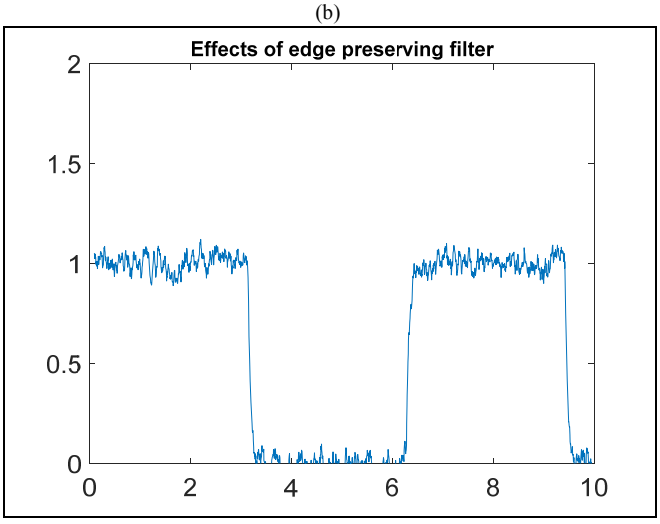

(c)

Figure 2. Example: the conceptual cross-section of the obstacle on the wall and the effects of the filtering with the EMA filter (a) ideal desired measurement of the depth; (b) real measurement of the depth with high noise and artefacts; (c) effects of the edge-preserving EMA

Fuzzy rule–based systems make soft decisions on each condition, then aggregate the decisions made, and finally make decisions based on aggregation. It must be emphasized that, in the literature an existing function had already been created [37] page [150], to automatically generate the IF-THEN rules and create a fuzzy system for provided input and output membership functions without any intervening steps. These functions were used in this research too.

The first step is to define the input membership functions that represent the gray intensity levels of the depth image after the edge-preserving filtering [33], [37] page [156], [38]. The obstacle is the brightest object in the depth image (the close objects are bright-white, the far objects are dark-black according to the RealSense camera)) because it is the closest object to the RealSense camera and all the other contents of the image are considered as the background in the image. Due to noise and artefacts, the background is not ideally dark-black, than it is variegated. These variations of gray intensities will later cause difficulties in the obstacle detection and extraction. There are three membership functions in the input of the fuzzy system, two trapezoidal and one triangular (Fig. 3. (a)). They were set after intensive experimentation to cover appropriately all the areas of the grayscale depth image. The blue trapezoidal function covers the area from black to bright gray levels, the red triangular function covers the middle area of gray levels and the orange trapezoidal function covers the highly bright levels in the image.

At the output, Bell type membership function has been selected to describe the output gray levels. As it can be seen, the first two input intervals are reduced at the output in two narrow intervals (blue and red functions) to transform the concerned input gray levels to dark gray levels. The third input is transformed in the narrow output (orange function) to emphasize the bright, white intensities of the obstacle as much as possible (Fig. 3. (b)).

Finally, the obtained fuzzy system is shown in Fig. 3 (c) [33], [37 - 38].

Thus, the obtained, enhanced depth image will contain a uniform darker background and a bright obstacle. This result will make it possible to extract the desired obstacle reliably from the EMA filtered depth image.

After the fuzzification followed by the binarization, the morphological functions are applied to extract the desired obstacles. The morphological connected components analysis is combined with morphological filtering using erosion operation [33], [37] pages [486-534], [38].

The problem of the occurrence of variable contrast is mostly avoided with camera's measurement parameter tune-up during the depth measurement and recording in the RealSense software stereo module [7 – 11]. There are many built-in parameters related to depth measurement such as depth visualization settings and built-in automatic histogram equalization. Thus, these settings avoid the need of automatic *t* threshold settings, because the recorded depth image will not have a large contrast variability after the tuning inside the RealSense software. All these parameters can be tuned via ROS system by user.

VII. Experiments and Results

In this section the experiments and their results will be explained in detail. The experiments were conducted with the RealSense D415 depth camera. The measurements were performed at the distance of 1m from the wall since the aim was to capture wide surface on the wall that would potentially need to be painted. The results are recorded as a point cloud with all necessary parameters: RGB matrix and the XYZ spatial coordinates matrix.

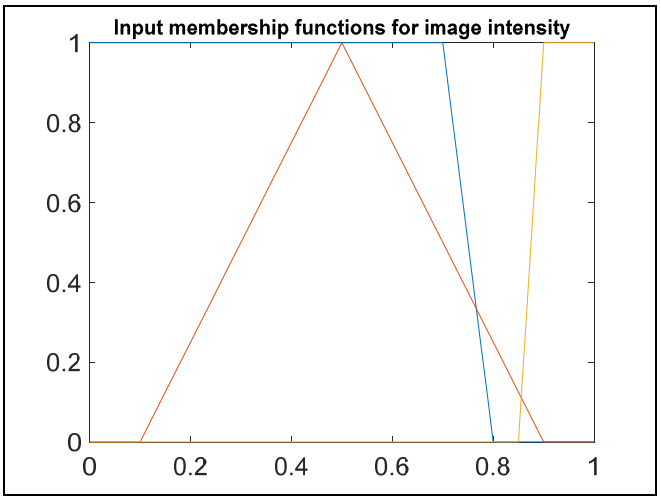

(a)

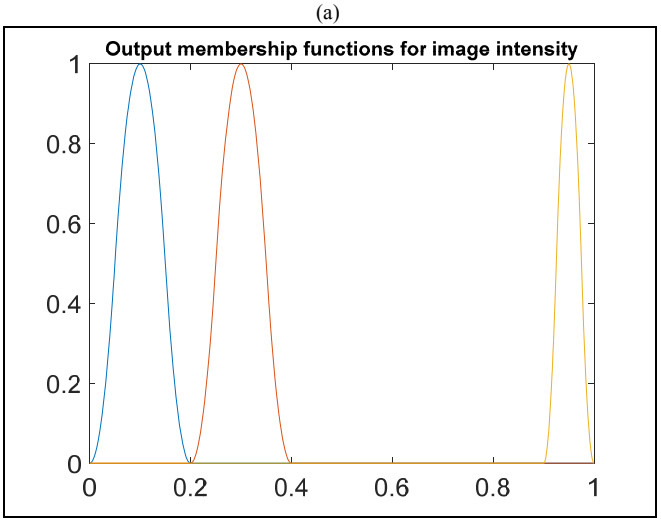

(b)

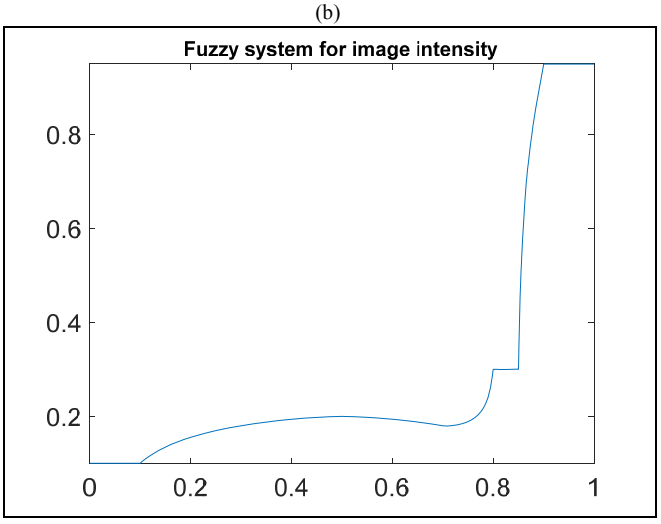

(c)

Figure 3. Development of the fuzzy system: (a) input membership functions; (b) output membership functions; (c) fuzzy inference system

Fig. 4. shows the images captured with the D415 camera. Fig. 4 (a) shows an obstacle of an undefined shape hanging on the wall, because the aim of the experiment is to explore the capabilities of the camera. It is important to note that the resolution of the RGB and depth cameras was set to the very maximum, i.e. to 1280x720 pixels and the so-called default mode of recording was used, which offers the best visual experience according to the manufacturer's specification, but this capturing mode does not use any post-processing (Fig. 4. (b)). It can be observed that the object of interest is clearly discernible in the depth image, but the image is blurred, and the background illumination is highly nonuniform. All these make extraction of the obstacle a difficult task. Further, the previously discussed post-processing techniques will be applied.

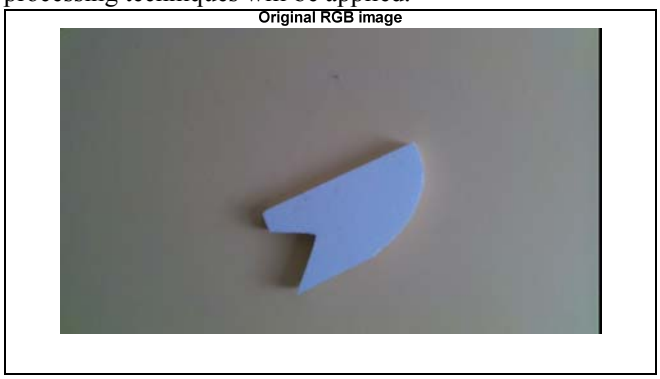

(a)

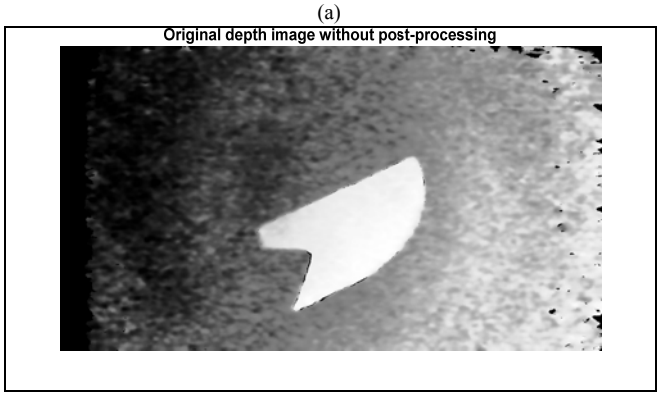

(b)

Figure 4. The image of the D415 camera with default settings: (a) RGB image; (b) depth image without post-processing

In the next step, the EMA edge-preserving filter was applied on the measured depth image.

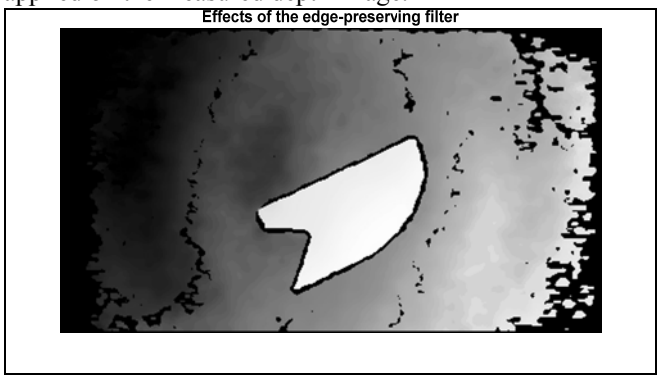

(a)

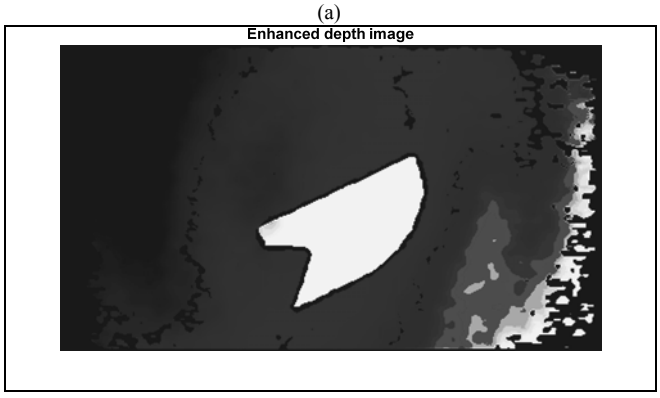

(b)

Figure 5. The image of camera D415 after post-processing: (a) effects of the edge-preserving filter; (b) effects of the fuzzy contrast enhancement

It should be noted that this filter is built-in in the RealSense software and it was applied through the camera wrapper. The filter parameters were set in the wrapper in order to obtain the best result. The tests showed that the best results were obtained for the values of $\alpha = 0.4$ and $\delta_{thresh} = 4$. Fig. 5. (a) shows the result of the edge-preserving filtering with the EMA filter. The edges, contours of the shape are well preserved and highlighted in the depth image. Still, the background is very non-uniform. Next, the fuzzy enhancement was applied in order to eliminate the illumination variations around the obstacle (Fig. 5. (b)). Fig. 6 (a) shows the result of the thresholding of the fuzzy enhanced image. This was necessary in order to apply the final morphological operations. Finally, using morphological connected component analysis and morphological filtering, the desired obstacle has been extracted from the depth image. The final result is shown in Fig. 6 (b).

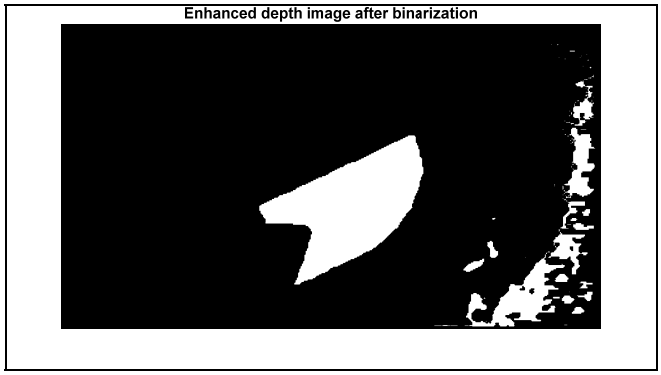

(a)

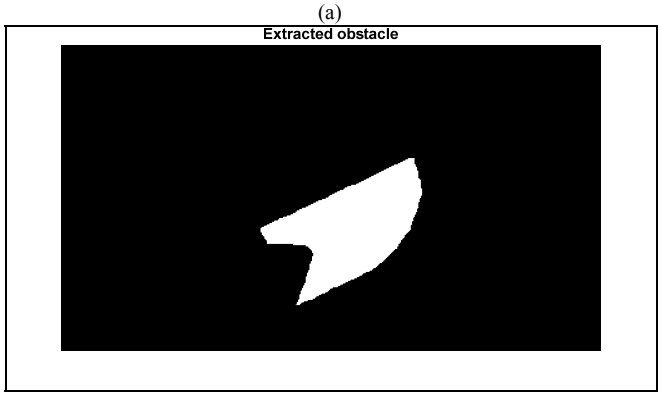

(b)

Figure 6. (a) Result of the binarization; (b) extracted obstacle after morphological filtering

Finally, the information about the extracted obstacle is forwarded to the robot's operating system in order to process the coordinates of the obstacle to avoid it during the painting process.

The next example presents a real situation where the wall should be separated from the window. The measurements were performed at the distance of 1m from the wall, again. The camera settings were the same as in the previous example. The image was captured at daylight under good lighting conditions. Strong sunrays are present on the right side. There is also a glare from the window glass because of the sunlight. In the upper left corner of the image is a shadow caused by the roof of the building. The experiment was performed outside on the first floor of the building on the terrace.

(a)

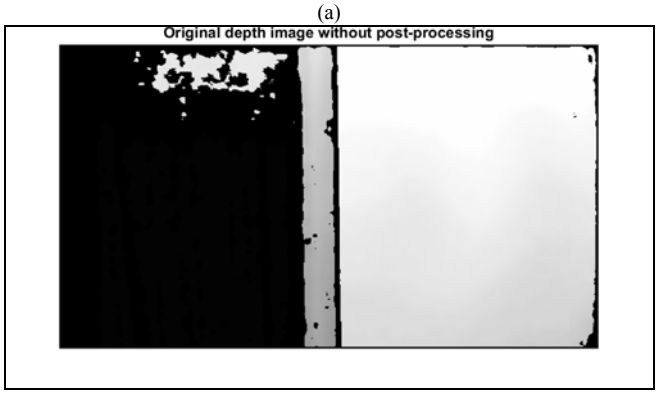

(b)

Figure 7. The image of the D415 camera with default settings: (a) RGB image; (b) depth image without post-processing

Fig. 7 (a) shows the original RGB image, while Fig. 7 (b) shows the original depth image without post-processing. In this example, the recorded original depth image is of very good quality. The border between the wall and window is clearly discernible due of the 8cm depth difference.

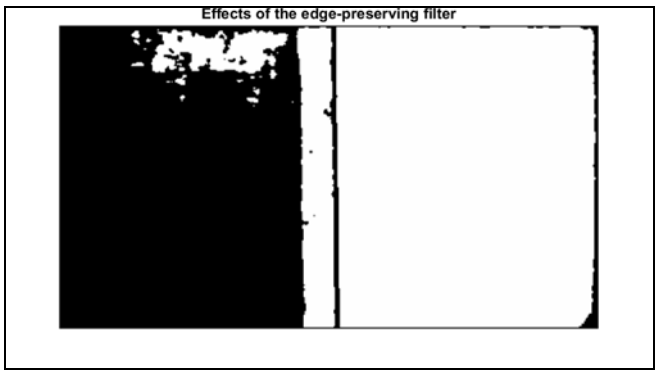

(a)

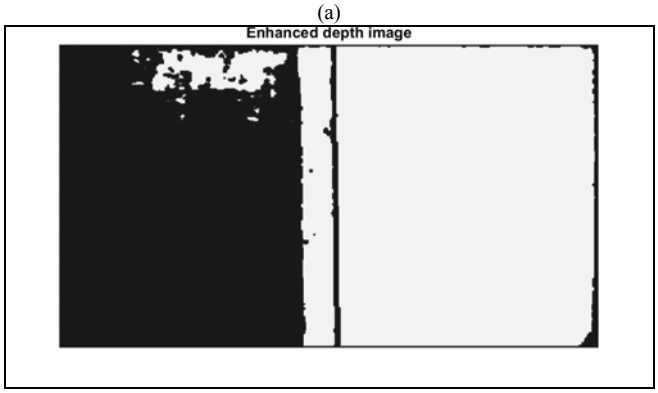

(b)

Figure 8. The image of camera D415 after post-processing: (a) effects of the edge-preserving filter; (b) effects of the fuzzy contrast enhancement

In the previous example, the depth difference between the obstacle and wall was 5cm. Since the depth difference is higher in the example from Fig. 7 (a), the resulted

measurements yielded in more clearly detected depth border in Fig. 7 (b).

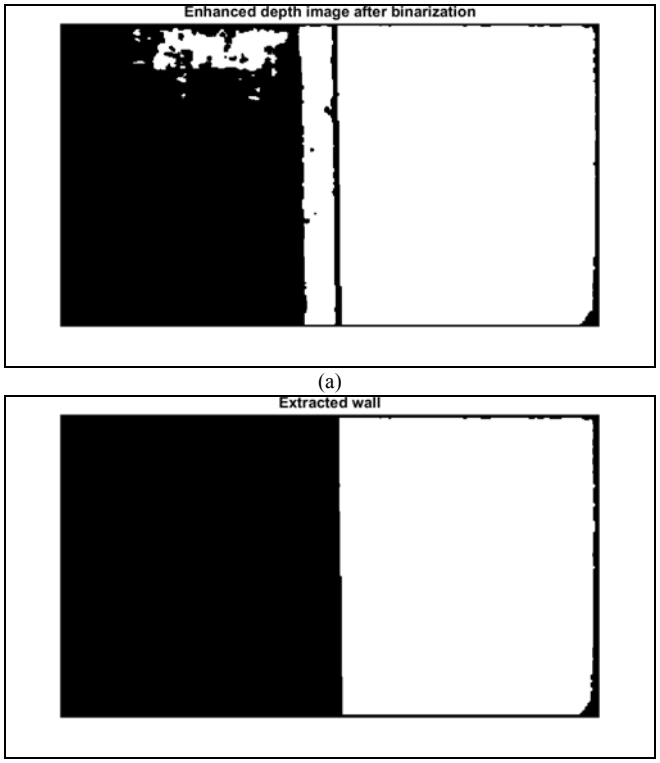

(a)

(b)

Figure 9. (a) Result of the binarization; (b) extracted obstacle after morphological filtering

Fig. 8 (a) presents the result of EMA edge-preserving filtering. As it can be seen, the filter sharpened and aligned the edges in the image. Fig. (b) displays the result of fuzzy contrast enhancement. Since the original depth image is of excellent quality, the fuzzy enhancement made a little improvement in the edge filtered image.

Finally, Fig. 9 (a) shows the results of binarization of the fuzzy enhanced image and Fig. 9 (b) displays the extracted wall are that should be painted. Again, the information about the extracted wall is forwarded to the robot's operating system in order to process the coordinates of the wall [42-48].

The ROS environment and corresponding software packages [49-54] were executed on a desktop computer characterized by an 8th Generation Intel® Core™ i7 processor (model No. i7-8700K), 32GB DDR4 RAM memory, GeForce GTX 1050 graphics card and 250 GB SSD drive. The image processing software finished all the pre- and processing steps in quite fast fashion involving couple of seconds wait time on the aforementioned hardware setup.

In the ROS environment, the robot kinematics and dynamics are implemented in a Unified Robot Description Format (URDF) file [55 – 61]. This file contains the joints locations, link parameters, limits and frames that describe the whole kinematic chain of the robot. At the end of defined kinematic chain, the camera frame is attached via a static transform publisher node. The transformations between different frames, e.g. between the reference coordinate and camera frames, are maintained with the tf ROS package, which enables the user to keep track of multiple coordinate frames over time. Once the camera stream is recorded, it is automatically transformed to the reference coordinate frame with the help of the aforementioned package. The accuracy of reference coordinate tracking depends on the controllers that keep the robot mechanism in closed loop. In this application, 0.005 m accuracy is satisfied by the controllers for the desired position tracking, and 0.01 rad accuracy is maintained for the desired orientation tracking.

Fig. 10 shows a screenshot from the Robotic Operating System visualization tool (Rviz) during the algorithm testing. The Rviz plugin is a part of the Robotic Operating System. This is a ROS graphical interface that allows to users to visualize a lot of information.

VIII. CONCLUSION

In the present paper, the working principle and the properties of Intel's RealSense depth cameras are briefly described. Appropriate experiments were conducted with the D415 camera and the evaluation of the experiments was performed. The aim of the experiments was to show the joint effectiveness of the EMA edge-preserving filter and the fuzzy contrast enhancement procedure for robotic applications. It was shown that the improvement of the depth image is significant relative to the depth images without post-processing, and thus the obstacles can easily be detected and extracted from the depth image recorded by the depth camera.

FUTURE WORK

In future, the depth camera will be embedded in the robot and the depth images will be captured during robot movements. The proposed obstacle detection procedure is planned be applied and tested in these dynamic conditions. Special emphasis will be placed on developing automated procedures for selecting particular obstacles from complex depth images in order to tune the robot for obstacle avoidance.

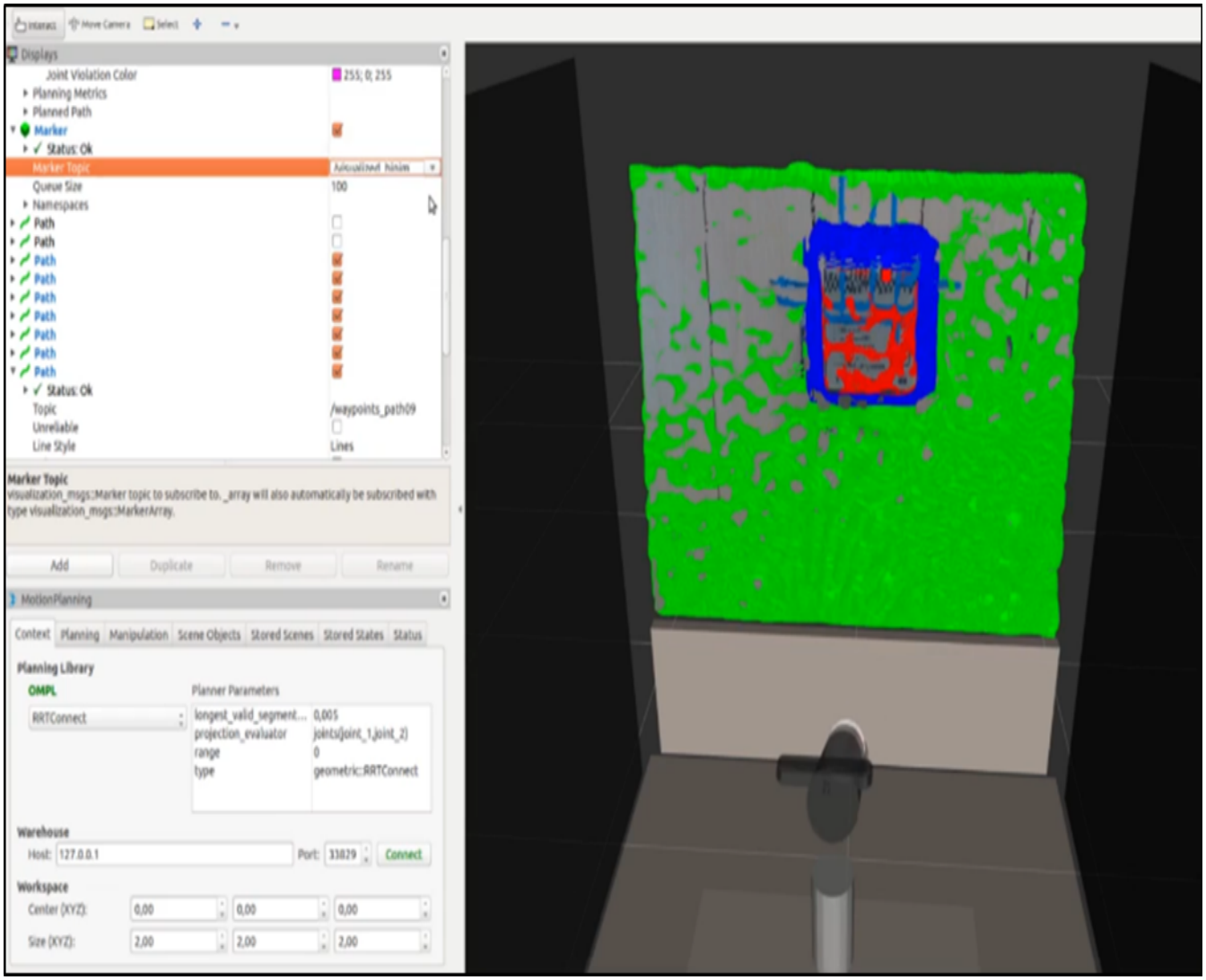

Figure 10. Screenshot from Robotic Operating System visualization tool (Rviz)

REFERENCES

[1] M. Carfagni, R. Furferi, L. Governi, C. Santarelli, M. Servi, "Metrological and Critical Characterization of the Intel D415 Stereo Depth Camera", Sensors, 2019, 19, 489; doi: 10.3390/s19030489.

[2] J. Hu, Y. Niu, Z. Wang, "Obstacle Avoidance Methods for Rotor UAVs Using RealSense", 2017, Chinese Automation Congress (CAC), doi: 10.1109/CAC.2017.8244068.

[3] S. Giancola, M. Valenti, R. Sala, "A Survey on 3D Cameras: Metrological Comparison of Time-of-Flight, Structured-Light and Active Stereoscopy Technologies", SpringerBriefs in Computer Science, Springer, ISSN 2191-5768, 2018, doi: 10.1007/978-3-319-91761-0.

[4] L. Keselman, J. I. Woodfill, A. Grunnet-Jepsen, A. Bhowmik, "Intel RealSense Stereoscopic Depth Cameras", 2017 IEEE Conference on Computer Vision and Pattern Recognition Workshops, doi: 10.1109/cvprw.2017.167.

[5] R. L. Lagendijk, R. E.H. Franich, E. A. Hendriks, "Stereoscopic Image Processing", The work was supported in part by the European Union under the RACE-II project DISTIMA and the ACTS project PANORAMA, doi: 10.1201/9781420046090-c22.

[6] F. L. Siena, B. Byrom, P. Watts, P. Breedon, "Utilising the Intel RealSense Camera for Measuring Health Outcomes in Clinical Research", Journal of Medical Systems (2018) 42: 53, doi: 10.1007/s10916-018-0905-x.

[7] "Intel RealSense D400 Series Product Family Datasheet", New Technologies Group, Intel Corporation, 2019, Document Number: 337029-005.

[8] A. Grunnet-Jepsen, D. Tong, "Depth Post-Processing for Intel RealSense D400 Depth Cameras", New Technologies Group, Intel Corporation, 2018, Rev 1.0.2, Article ID 000028866.

[9] "Evaluating Intel's RealSense SDK 2.0 for 3D Computer Vision Using the RealSense D415/D435 Depth Cameras", 2018, Berkeley Design Technology, Inc.

[10] "Intel RealSense Camera Depth Testing Methodology", New Technologies Group, Intel Corporation, 2018, Revision 1.0.

[11] A. Grunnet-Jepsen, J. N. Sweetser, J. Woodfill, "Best-Known-Methods for Tuning Intel RealSense D400 Depth Cameras for Best Performance", New Technologies Group, Intel Corporation, Rev 1.9, Article ID 000027833.

[12] E. S. L. Gastal, M. M. Oliveira, "Domain Transform for Edge-Aware Image and Video Processing", ACM Transactions on Graphics, Volume 30 (2011), Number 4, Proceedings of SIGGRAPH 2011, doi: 10.1145/2010324.1964964.

[13] A. Grunnet-Jepsen, P. Winer, A. Takagi, J. Sweetser, K. Zhao, T. Khuong, D. Nie, J. Woodfill, "Using the Intel RealSenseTM Depth cameras D4xx in Multi-Camera Configurations", New Technologies Group, Intel Corporation, Rev 1.1, Article ID 000028140

[14] "Intel RealSense Depth Module D400 Series Custom Calibration", New Technologies Group, Intel Corporation, 2019, Revision 1.5.0, Article ID 000026725

[15] A. Grunnet-Jepsen, J. N. Sweetser, "Intel RealSens Depth Cameras for Mobile Phones", New Technologies Group, Intel Corporation, 2019, Article ID 000026983

[16] P. Krejov, A. Grunnet-Jepsen, "Intel RealSense Depth Camera over Ethernet", New Technologies Group, Intel Corporation, 2019

[17] J. Cunha, E. Pedrosa, C. Cruz, A. J. R. Neves, N. Lau, "Using a Depth Camera for Indoor Robot Localization and Navigation", Conference: RGB-D Advanced Reasoning with Depth Cameras Workshop, Robotics Science and Systems Conference (RSS), At LA, USA, 2011

[18] H. J. Hemmat, E. Bondarev, P. H. N. de With, "Real-time planar segmentation of depth images: from 3D edges to segmented planes",

Journal of Electronic Imaging 24(5): 051008, 2015, doi: 10.1117/1.JEI.24.5.051008.

[19] F. Flacco, T. Kroger, A. De Luca, O. Khatib, "A depth space approach to human-robot collision avoidance" 2012, IEEE International Conference on Robotics and Automation, doi: 10.1109/icra.2012.6225245

[20] A. Saxena, S. H. Chung, A. Y. Ng, "3-D Depth Reconstruction from a Single Still Image", International Journal of Computer Vision, 2008, Volume 76, Issue 1, pp 53–69, doi: 10.1007/s11263-007-0071-y

[21] V. Sterzentsenko, A. Karakottas, A. Papachristou, N. Zioulis, A. Doumanoglou, D. Zarpalas, P. Daras, "A low-cost, flexible and portable volumetric capturing system", 14th International Conference on Signal-Image Technology & Internet-Based Systems, 2018, doi: 10.1109/SITIS.2018.00038

[22] N. Carey, R. Nagpal, J. Werfel, "Fast, accurate, small-scale 3D scene capture using a low-cost depth sensor", 2017 IEEE Winter Conference on Applications of Computer Vision (WACV), doi: 10.1109/WACV.2017.146

[23] C. Garnica, F. Boochs, M. Twardochlib, "A New Approach To Edge-Preserving Smoothing for Edge Extraction and Image Segmentation", International Archives of Photogrammetry and Remote Sensing. Vol. XXXIII, Part B3. Amsterdam 2000.

[24] S. Reich, F. Wörgötter, B. Dellen, "A Real-Time Edge-Preserving Denoising Filter'' In Proceedings of the 13th International Joint Conference on Computer Vision, Imaging and Computer Graphics Theory and Applications, 2018), Vol. 4: VISAPP, pages 85-94, doi: 10.5220/0006509000850094

[25] R. Abiko, M. Ikehara, "Fast Edge Preserving 2D Smoothing Filter Using Indicator Function", ICASSP 2019, 978-1-5386-4658-8/18, IEEE, doi: 10.1109/ICASSP.2019.8683544

[26] J. Choi, H. Park, D. Seo, "Pansharpening Using Guided Filtering to Improve the Spatial Clarity of VHR Satellite Imagery", Remote Sensing, 2019, 11, 633; doi: 10.3390/rs11060633

[27] N. Iqbal, S. Ali, I. Khan, B. M. Lee, "Adaptive Edge Preserving Weighted Mean Filter for Removing Random-Valued Impulse Noise", Symmetry 2019, 11, 395; doi: 10.3390/sym11030395

[28] F. Zhu, Z. Liang, X. Jia, L. Zhang, Y. Yu, "A Benchmark for Edge-Preserving Image Smoothing", IEEE Transactions on Image Processing 28(7): 3556-3570, 2019, doi: 10.1109/TIP.2019.2908778

[29] J. Sandeep, K. Samrudh, "Image contrast enhancement using fuzzy logic", arXiv: 1809.04529, 2018.

[30] D. Van De Ville, M. Nachtegael, D. Van der Weken, E. E. Kerre, W. Philips, I. Lemahieu, "Noise reduction by fuzzy image filtering", IEEE Transactions on Fuzzy Systems, 11(4), 429–436. doi: 10.1109/tfuzz.2003.814830

[31] H. D. Cheng, H. Xu, "A novel fuzzy logic approach to contrast enhancement", Pattern Recognition Volume 33, Issue 5, May 2000, Pages 809-819, doi: 10.1016/s0031-3203(99)00096-5

[32] A. S. Parihar, O. P. Verma, C. Khanna, "Fuzzy-Contextual Contrast Enhancement", IEEE Transactions on Image Processing, Volume: 26 , Issue: 4 , April 2017, doi: 10.1109/TIP.2017.2665975

[33] V. Tadic, M. Popovic, P. Odry, "Fuzzified Gabor filter for license plate detection", Engineering Applications of Artificial Intelligence, 2016, 48, 40–58, doi: 10.1016/j.engappai.2015.09.009

[34] A. A. M. Salih, K. Hasikin, N. A. M. Isa, "Adaptive Fuzzy Exposure Local Contrast Enhancement", IEEE Access, Volume: 6, 58794 – 58806, doi: 10.1109/ACCESS.2018.2872116

[35] A. S. Parihar, "Fuzzy adaptive gamma correction for contrast enhancement", 2017 International Conference on Intelligent Sustainable Systems (ICISS), IEEE 2018, doi: 10.1109/ISS1.2017.8389246

[36] V. Tadic, A. Odry, I. Kecskes, E. Burkus, Z. Kiraly, P. Odry, "Application of Intel RealSense Cameras for Depth Image Generation in Robotics", WSEAS Transactions on Computers, E-ISSN: 2224-2872, Volume 18, 2019

[37] R.C. Gonzales, R.E. Woods, S.L. Eddins, "Digital Image Processing Using MATLAB", pp. 150-156 and 486-534, 2nd Edition, Gatesmark, LLC, USA, 2009, ISBN-13: 978-0982085400

[38] V. Tadic, Z. Kiraly, P. Odry, Z. Trpovski, T. Loncar-Turukalo, "Comparison of Gabor Filter Bank and Fuzzified Gabor Filter for License Plate Detection", Acta Polytechnica Hungarica, 17(1): 61-81, 2020, doi: 10.12700/APH.17.1.2020.1.4

[39] NIST/SEMATECH e-Handbook of Statistical Methods, http://www.itl.nist.gov/div898/handbook/, 2012.

[40] J. S. Hunter, "The Exponentially Weighted Moving Average", Journal of Quality Technology, 18:4, 203-210, 1986, doi: 10.1080/00224065.1986.11979014

[41] T. Chaira, A. K. Ray, "Fuzzy Image Processing and Applications with MATLAB", pp. 47-49, CRC Press, Taylor & Francis Group, LLC, USA, 2009.

[42] P. M. Khandekar, S. S. Chiddarwar, A. Jha, "Programming of an Industrial Robot Using Demonstrations and Soft Computing Techniques", Journal of Scientific & Industrial Research, pp. 156-163, Vol. 77, 2018

[43] D. Ristić-Durrant, S. M. Grigorescu, A. Gräser, Ž. Ćojbašić, V. Nikolić, "Robust Stereo-Vision Based 3D Object Reconstruction for the Assistive Robot FRIEND", Advances in Electrical and Computer Engineering, Volume 11, Number 4, 2011, doi: 10.4316/AECE.2011.04003

[44] X. Ning, G. Tian, Y. Wang, "Top-Down Approach to the Automatic Extraction of Individual Trees from Scanned Scene Point Cloud Data", Advances in Electrical and Computer Engineering, Volume 19, Number 3, 2019, doi: 10.4316/AECE.2019.03002

[45] E. Asadi, B. Li, I. M. Chen, "Pictobot: A Cooperative Painting Robot for Interior Finishing of Industrial Developments with High Walls", IEEE Robotics & Automation Magazine, 2018, doi: 10.1109/MRA.2018.2816972

[46] I. M. Chen, E. Asadi, J. Nie, R. J. Yan, W. C. Law, E. Kayacan, S. H. Yeo, K. H. Low, G. Seet, R. Tiong, "Innovations in Infrastructure Service Robots", CISM International Centre for Mechanical Sciences 2016, doi: 10.1007/978-3-319-33714-2_1

[47] L. Somlyai, Z. Vámossy, "SLAM algorithm for mobile robot localization with RGB-D camera", Fluids, Heat and Mass Transfer, Mechanical and Civil Engineering, WSEAS, ISBN: 978-1-61804-358-0

[48] G. Kertesz, S. Szenasi, Z. Vamossy, "Multi-Directional Image Projections with Fixed Resolution for Object Matching", Acta Polytechnica Hungarica, Vol. 15, No. 2, 2018, doi: 10.12700/aph.15.1.2018.2.11.

[49] T. Haidegger, G. S. Virk, C. Herman, R. Bostelman, P. Galambos, Gy. Györök, I. J. Rudas, "Industrial and Medical Cyber-Physical Systems: Tackling User Requirements and Challenges in Robotics", Recent Advances in Intelligent Engineering, vol 14. Springer, Cham, 2020, doi: 10.1007/978-3-030-14350-3_13.

[50] A. R. Várkonyi-Kóczy, A. Rövid, "Soft Computing Based Point Correspondence Matching for Automatic 3D Reconstruction", Acta Polytechnica Hungarica, Vol. 2, No. 1, 2005.

[51] E. Burkus, P. Odry, "Autonomous Hexapod Walker Robot "Szabad(ka)"", Acta Polytechnica Hungarica, Vol. 5, No. 1, 2008.

[52] R. Szabó, A. Gontean, "Robotic Arm Control Algorithm Based on Stereo Vision Using RoboRealm Vision", Advances in Electrical and Computer Engineering, Volume 15, Number 2, 2015, doi: 10.1109/CACS.2013.6734114

[53] I. Kecskés, E. Burkus, F. Bazsó, P. Odry, "Model validation of a hexapod walker robot", Robotica 35, no. 2, 2017, pp. 419-462, doi: 10.1017/S0263574715000673

[54] A. Koubaa, "Robot Operating System (ROS)", Springer International Publishing Switzerland 2016, doi: 10.1007/978-3-319-26054-9

[55] J. Kramer, M. Scheutz, "Development environments for autonomous mobile robots: A survey", Autonomous Robots, vol. 22, no. 2, pp. 101–132, 2007.

[56] G. Bradski, A. Kaehler, "Learning OpenCV", pp. 115-124, O'Reilly Media, Inc., 1005, USA, ISBN: 978-0-596-51613-0, 2008

[57] A. Martinez, E. Fernández, "Learning ROS for Robotics Programming", pp. 63-102, Published by Packt Publishing Ltd., UK., 2013, ISBN 978-1-78216-144-8

[58] J. Kerr, K. Nickels, "Robot operating systems: Bridging the gap between human and robot", Proceedings of the 44th Southeastern Symposium on System Theory (SSST), doi: 978-1-4577-1493-1/12, 2012

[59] V. Tadić, E. Burkus, A. Odry, I. Kecskes, Z. Kiraly, P. Odry, "Effects of the Post-processing on Depth Value Accuracy of the Images Captured by RealSense Cameras", Contemporary Engineering Sciences, Vol. 13, 2020, no. 1, 149 – 156, HIKARI Ltd, doi: 10.12988/ces.2020.91454

[60] M. Quigley, B. Gerkey, W. D. Smart, "Programming Robots with ROS", pp. 391-394, O'Reilly Media, Inc., 2015, ISBN: 978-1-4493-2389-9

[61] V. Tadic, A. Odry, A. Toth, Z. Vizvari, P. Odry, "Fuzzified Circular Gabor Filter for Circular and Near-Circular Object Detection", IEEE Access, doi: 10.1109/ACCESS.2020.2995553